High precision open-loop and closed-loop MEMS accelerometers with wide sensing range

Boris Grinberg, Aviram Feingold, Leonid Furman, Roza Wolfson
Physical Logic LTD
Israel
boris@physical-logic.com

Abstract — **This paper presents two high performance wide sensing range MEMS accelerometers, built using different techniques. The paper comprises two sections. In the first section, open-loop accelerometers with up to 40 g sensing range and 18 bit dynamic range are presented. In addition to a discussion on design, statistically based test results are demonstrated. In the second section, a closed-loop sigma-delta accelerometer with 30 g sensing range and 21 bit dynamic range is presented, including a short design review and test results from the most recently fabricated batches.**

Our open-loop accelerometers have demonstrated tactical grade performance featuring 0.5 ppm of full range/√Hz noise, 100 ppm bias stability, and 0.5 % of full range nonlinearity. Our closed-loop accelerometer, designed to compete with traditional macro electro-mechanical quartz accelerometers, features <10 μg bias instability, 0.1% typical nonlinearity over full 30 g sensing range, and less than 100 $\mu g/g^2_{rms}$ Vibration Rectification Error (VRE) up to a 2 kHz frequency range.

Both open-loop and closed-loop sensors represent a fully integrated system comprising a uniquely designed MEMS device enclosed in a specially built LCC package with a proprietary ASIC.

Keywords—MEMS accelerometer; closed/open-loop; tactical/navigation grade; sigma-delta

I. INTRODUCTION

High performance capacitive MEMS accelerometers are increasingly being used in various motion sensing applications including medical [1,2], industrial, and military requiring measurement of acceleration, vibration, shock, tilt, rotation etc. In a wide range of inertial navigation applications, tactical grade MEMS accelerometers are already the preferred solution due to their small size, low power consumption, and convenient price; however, in Inertial Measurement Units (IMU) and Inertial Navigation Systems (INS) which are designed for navigation grade applications, conventional non-MEMS accelerometers are generally used, such as electro-mechanical servo and bulk piezoelectric accelerometers. During the past decade, design and initial measurement results of closed-loop MEMS accelerometers were presented [5-9], showing the potential of the MEMS technology to deliver a smaller and cheaper sensor while realizing inertial navigation grade performance.

In order to achieve navigation grade performance, high linearity (<0.1%) is an important parameter to satisfy. Linearity may be limited by the capacitive nature of MEMS sensors in which output is inversely proportional to the gap change in the sense capacitor [8]. Closed-loop MEMS accelerometers, which use electrostatic force feedback, balance the sensor structure around its nominal position, neutralizing the influence of the sense capacitor nonlinearity. There is a variety of system design challenges towards attaining navigation-grade level. Firstly, a linear and stable feedback pass must be established. In addition to the improved linearity, other parameters such as short and long term bias, scale factor stability, and Vibration Rectification Error (VRE) need to be addressed from the design level in order to satisfy all the requirements during the integration of the sensor system.

Physical Logic first presented its tactical grade MAXL-OL-2000 open-loop MEMS accelerometer series and its navigation grade MAXL-CL-3030 sigma-delta MEMS accelerometers in 2015 [9]. These accelerometers are designed with special in-plane bulk micromachining technology, in order to achieve improved performance over a wide sensing range. This paper expands the discussion on the open-loop accelerometer design and reports more measurement results in part II. In part III, along with the discussion on design, we disclose the most recent measurement results from our closed-loop sensor.

II. OPEN-LOOP ACCELEROMETERS

A. System architecture

Physical Logic's MAXL-OL-2000 open-loop accelerometer is comprised of a spring-mass MEMS and a signal conditioning ASIC (see Fig. 2). The ASIC represents an integrated chip which includes an Analog Front End (AFE) for capacitance to voltage conversion, a Power Management (PM) section, a clock generation section, and an analog temperature sensor. The MEMS device is arranged such that it forms a full-bridge configuration of four sense capacitors, enabling differential input signal to the AFE. The AFE is implemented in a continuous-time transcapacitance topology with chopper stabilization and a Low Pass Filter (LPF) which limits the output signal bandwidth. The power management section provides all regulated supplies and reference voltages used in the sensor. The clock generation section consists of an oscillator core and is responsible for providing the chopping clock. The temperature sensor provides an analog temperature measurement for system level calibration.

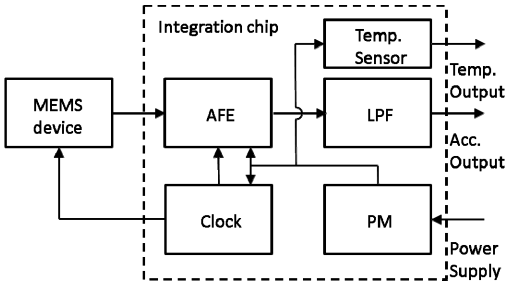

Fig. 1. Open-loop accelerometer system diagram.

The dynamics of the MEMS device is that of a traditional damped spring-mass system with the relation between external acceleration a and the proof mass displacement relative to the accelerometers frame x governed by (1).

$$m\frac{d^2x}{dt^2}+b\frac{dx}{dt}+kx=ma\,, \qquad (1)$$

where m is the mass of the proof mass, b is the damping coefficient, and k is the spring coefficient. Or, equivalently,

$$\frac{d^2x}{dt^2}+\frac{\omega_0}{Q}\frac{dx}{dt}+\omega_0^2x=a\,, \qquad (2)$$

where $\omega_0=\sqrt{k/m}$ is the natural angular frequency, and $Q=\omega_0 m/b$ is the quality factor. At frequencies much lower than the natural frequency, the relationship can be simplified as follows:

$$x=\frac{a}{\omega_0^2}. \qquad (3)$$

The process of capacitance to voltage conversion in MAXL-OL-2000 accelerometers can be described by a simplified electronic scheme shown in Fig. 2. Applying external acceleration causes a displacement of the proof mass, which leads to a capacitance change in C_1 to C_4 bridge capacitors in accordance with the arrows in the figure. The capacitance change is then converted to a differential output voltage.

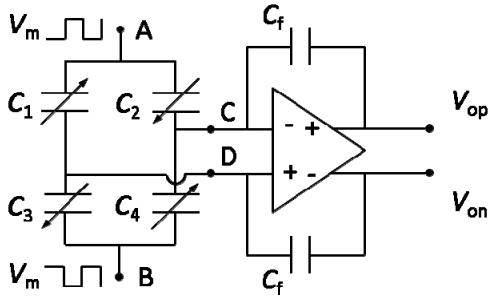

Fig. 2. Open-loop accelerometer system diagram.

Analyzing the scheme in Fig. 2, the capacitance to voltage conversion is derived as follows:

$$V_o=V_{op}-V_{on}=\{(C_1-C_3)+(C_4-C_2)\}\frac{V_m}{2C_f}\,, \qquad (4)$$

where V_o is the differential output voltage, V_m is the modulation reference voltage, C_f is the feedback capacitance of the AFE amplifier. Equations (3) and (4) govern how acceleration sensing is realized in the MAXL-OL-2000 accelerometer series.

B. MEMS design

In the design of the MEMS device for the open-loop accelerometer we chose an alternative to the conservative concept of out-of-plane bulk micro-machined sensor, described in [3]. In our patented design we use the advantages of bulk micro-machining processed on Silicon on Isolator (SOI) wafer to realize a massive proof mass (~1 miligram) with in-plane displacement [9]. The concept provides several critical advantages. It avoids the nonlinearity of the capacitance sensing based on gap-changing while allowing for implementation of a full bridge sensing topology with a large capacitor (4 x 6 pF) for more effective parasitic rejection. In addition, a highly symmetric mechanical geometry is realized in which each of the four sensing capacitors is equally distributed on the area of the MEMS die. The size of the proof mass also guarantees a low input referred thermo-mechanical noise (< 1.5 µg/√Hz) with no need for vacuum packaging.

The design of the MEMS device takes into consideration mechanical and electrical specifications along with the limitations of the fabrication process. After the design of the structure suspension and general geometry, the device is carefully modeled using Final Element (FEM) analysis tools. The modeling takes into consideration tolerances of the fabrication process and Eigen frequency analysis and damping estimation are performed. TABLE I. .These values were confirmed by measurement to be within <10% of the design.

The electrical design concentrates on optimizing the sense capacitor geometry for achieving better scale factor linearity. In order to better understand the process of electrical design it is essential to understand the topology of the MEMS device which is schematically shown in Fig. 3.

TABLE I. MECHANICAL DESIGN

	Accelerometer sensing range [g]				
	2	***5***	***10***	***20***	***40***
Sense mode Eigen frequency [Hz]	680	1075	1520	2152	3037
Next Eigen frequency [Hz] [Value/Direction]	4649/z	8020/z	10420/z	13020/z	14735/z
Quality factor	0.5	0.7	1	1.5	2

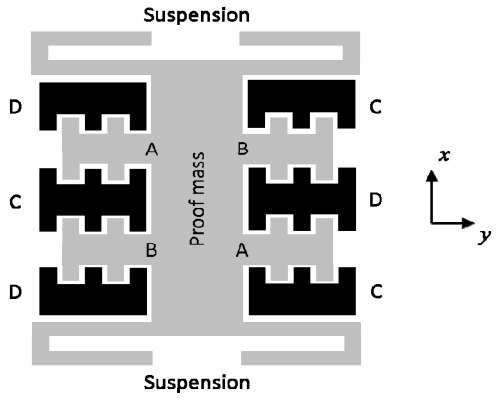

Fig. 3. MEMS device topology scheme (top view).

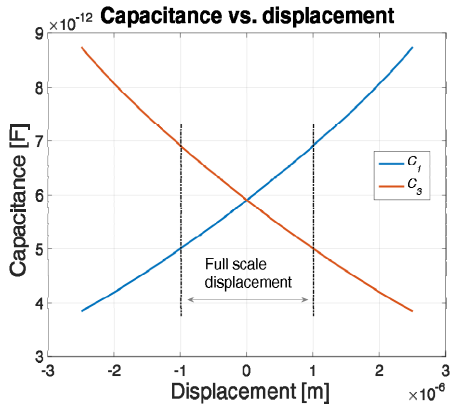

Fig. 4. Capacitance vs. displacement plot from FEM analysis.

Notice that electrical nodes A, B, C, and D are indicated in both Fig. 2 and Fig. 3. Capacitance of each of the four sense capacitors of the bridge can be modeled as a function of the proof mass displacement using FEM analysis (see Fig. 4). For the nonlinearity estimation one can assume that the geometry of the four sense capacitors is identical. In this case, (4) can be rewritten as

$$V_o = \left(C(x) - C(-x)\right)\frac{V_m}{C_f}, \tag{5}$$

indicating the dependence of the sense capacitors on the proof mass displacement. Performing a third order polynomial approximation for (5), we can evaluate second and third order nonlinearity coefficients which define the MEMS device nonlinearity error function $N(x)$ as follows:

$$\begin{aligned} h(x) &\equiv C(x) - C(-x), \\ \tilde{h}(x) &= P(x) = \sum_{i=0}^{3} a_i x^i, \\ N(x) &\equiv \frac{a_2}{a_1}x^2 + \frac{a_3}{a_1}x^3. \end{aligned} \tag{6}$$

The $P(x)$ in (6) represents the third order polynomial approximation for $h(x)$. The error function defined in (6) is generic for the open-loop accelerometers of any sensing range, since the proof mass displacement at accelerometer full scale, shown in Fig. 4, is identical in each design. Fig. 5 shows the nonlinearity error in percent, calculated by

$$Error\,[\%] = \frac{N(x)}{x}100. \tag{7}$$

As can be seen from the plot the contribution of the second order nonlinearity is minor as compared to the third order nonlinearity. The designed nonlinearity of the MEMS device is <0.5 % of the full scale. A more rigorous treatment would account for the fact that the capacitors of the MEMS device are not identical due to fabrication imperfections. Each of the four sense capacitors in a fabricated device goes through an electrical Capacitance-Voltage (CV) test, to evaluate the mismatch between the capacitors of the bridge as an acceptance test, before being assembled in the final product.

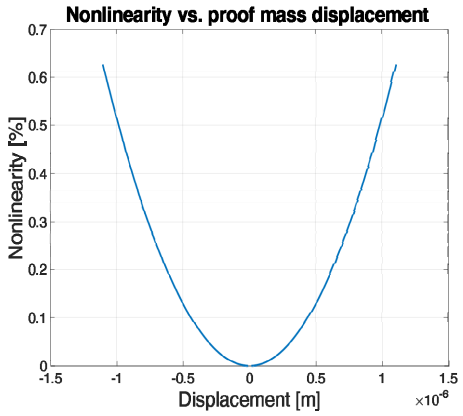

Fig. 5. Nonlinearity vs. proof mass displacement.

C. *ASIC integrated chip*

MAXL-OL-2000 accelerometer series comprises open-loop accelerometers with sensing range from 2 g to 40 g. The sensing range is defined by the mechanical design of the MEMS device. All the accelerometers of the series are assembled using a signal conditioning integrated chip which was specially designed to achieve high performance compatible with tactical grade inertial sensors. Along with the MEMS device, the ASIC chip plays a key role in achieving the accelerometers target specification. The implemented technology of the AFE is a continuous-time, transcapacitance topology which is relatively convenient to implement in CMOS technology and provides good noise performance. The detailed AFE design overview, including noise analysis, chopper stabilization verification, nonlinearity estimation and more, is presented in [4]. Our latest ASIC generation has been brought to its optimal performance, improving start-up time, Turn On to Turn On (TOTO) repeatability, linearity, and power consumption. The key parameters of the integrated chip used in MAXL-OL-2000 accelerometers are summarized in TABLE II.

TABLE II. ASIC PARAMETERS

Parameter Description	Unit	Specification Value	Measured Value
Output range	V	±1.5	-
Noise	nV/√Hz	<310	<50
Nonlinearity	% of ±1.2V range	<|0.2|	<|0.15|
Operation temperature range (OTR)	^{0}C	-40 to 85	-
Temperature coefficient (in OTR)	µV/^{0}C	<1	<0.5
Start-up time (in OTR)	msec	<200	<20
Turn on-to-turn on repeatability (in OTR)	µV	<40	<10
Power supply	V	3.3	-
Power supply sensitivity	µV/V	<30	<50
Power consumption	mW	<60	<45
Size	mm X mm	4.6 X 2	-

D. Open-loop accelerometers measurement results

We published a short overview of measurement results from MAXL-OL-2000 open-loop accelerometers in [9]. This overview contained temperature sensitivity and hysteresis, TOTO repeatability, and long term repeatability. In this paper we include additional information on such important parameters as noise, scale factor linearity, and short term stability. Both [9] and this paper concentrate for simplicity on measurement results of 20 g and 40 g range sensors.

- *Noise*: Fig. 6 shows a typical PSD measurement taken from the MAXL-OL-2040 accelerometer. Since the dominant contribution in the 300 Hz bandwidth comes from flicker noise, we can estimate the equivalent noise density of the sensor. The formula in (8) is based on calculating output signal RMS over the 0.1 Hz to 300 Hz frequency range, as if it was comprised of flicker noise only. The formula assumes 1st order low pass filter at 300 Hz.

$$Noise = K\sqrt{\frac{\ln 3000}{1.57\times 300}}. \qquad (8)$$

The K in (8) is the square root of the PSD value at 1 Hz. Fig. 7 shows the statistical monitor of the equivalent noise density based on the acceptance test results of MAXL-OL-2040 accelerometers fabricated in 2015. Each point on the plot represents a measured result from a different sensor. There is a clear improvement in results as the unit number grows, indicating the trend of stabilization in the fabrication process.

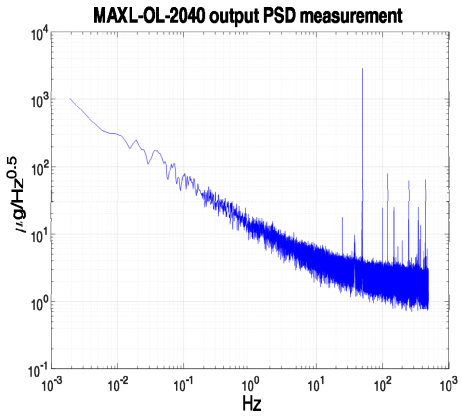

Fig. 6. MAXL-OL-2040 PSD plot

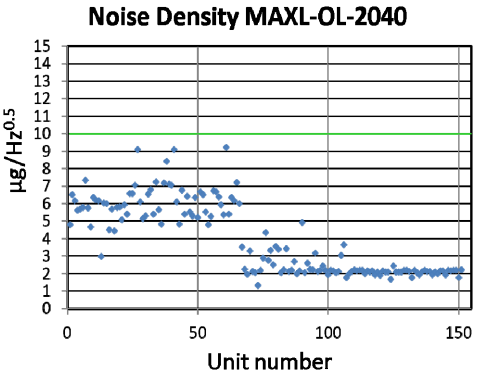

Fig. 7. MAXL-OL-2040 noise density statistical monitor

- *Short term stability*: Fig. 8 shows measurements taken from six MAXL-OL-2020 accelerometers for 18 hours in room temperature with no temperature control. Maximum bias deviation from the initial value is about 0.8 mg.

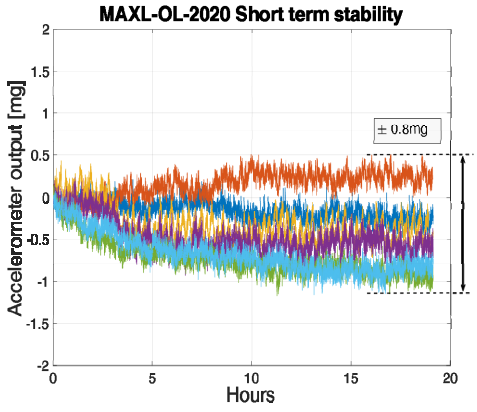

Fig. 8. MAXL-OL-2020 Short term stability

- *Linearity*: MAXL-OL-2040 accelerometers went through precise centrifuge testing for scale factor linearity evaluation. A typical linearity error is presented in Fig. 9. The error is calculated using a linear approximation based on 0 g and 1 g measurements. Summarizing the results from six sensors, a nonlinearity of 0.5% of the input acceleration in 35 g range is observed.

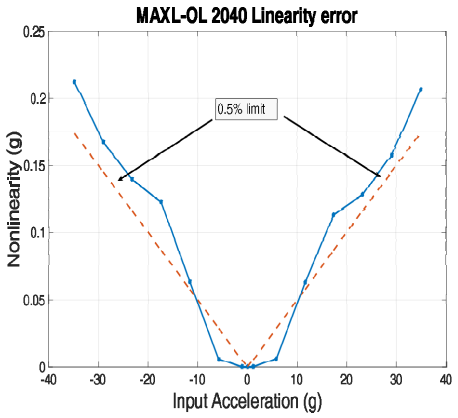

Fig. 9. MAXL-OL-2040 nonlinearity error

III. CLOSED-LOOP ACCELEROMETERS

MEMS accelerometer technology has clear advantages over macro electro-mechanical and quartz resonating accelerometers: size, weight, power consumption, robustness, and price. Nevertheless, bringing MEMS accelerometers to a level of performance compatible to that of the traditional navigation grade accelerometers appears to be quite challenging. In this chapter we disclose Physical Logic MAXL-CL-3030 30 g sensing range, closed-loop, sigma-delta MEMS accelerometer; whose performance proves that wide sensing range inertial navigation grade MEMS accelerometer is a reality.

A. System architecture

MAXL-CL-3030 accelerometer operates as a 4th order sigma-delta modulator used to convert external acceleration into a high frequency single bit digital signal. Sigma-delta modulation is a well-known technique in the field of A/D and D/A converters. Almost every high resolution low-frequency A/D converter is based on the sigma-delta modulation principle. This technique is well suited for low-frequency signals corresponding to the frequency band of acceleration signals. During the last 20 years sigma-delta modulation has also been applied to MEMS inertial sensors, allowing exploitation of its numerous advantages. In addition to the feedback linearization and the ability of utilizing digital compensation with a low resolution A/D converter, the technique provides an inherently high resolution digital output, thus suppressing the need for a high resolution A/D converter. All this comes, however, at the expense of increased system design complexity. The presence of the non-linear 1-bit comparator in the loop prohibits the use of classic linear control design, raising the need for careful numerical simulation in order to attain required stability and robustness [6]. Fig. 10 shows a schematic system diagram of our closed-loop accelerometer. Applying external acceleration causes mechanical displacement of the proof mass, which is detected and converted into analog voltage as is described in the previous chapter. The signal is then digitalized in a low resolution high frequency A/D converter before being processed in the digital loop compensator. The output of the compensator is put through the 1-bit sign comparator to get the single bit stream. This bit stream carries the acceleration signal information in a 1-bit format at highly oversampled ratio, which after decimation, corresponds to a high resolution digital signal in the required bandwidth. The signed 1-bit data coming out of the comparator is then fed back through a driver to generate an actuation force pulse on the MEMS sensor.

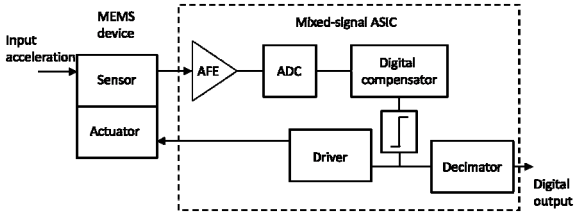

Fig. 10. Closed-loop system diagram

B. The main chalanges of system design

The design of sigma-delta MEMS accelerometers has been an active area of research for at least two decades. In [5] noise analysis of a sigma-delta micro-accelerometer was presented. A detailed system design with a focus on closed loop stability of a sigma-delta accelerometer with high-Q MEMS device is presented in [6]. In [8] we describe the system architecture of Physical Logic's sigma-delta MEMS accelerometer, providing a simulation based proof of concept. In this paper, we shortly overview the main system design challenges and focus on the measurement results.

- *Control loop stability*: The presence of a nonlinear 1-bit comparator in the control loop makes the task of control design, which provides a robust and stable operation over full sensing range of the accelerometer, more challenging. Although one can start with applying linear control theory techniques, the final design should be based on careful numerical simulation.

- *System clock*: The oscillator core that generates the system clock is the "heart" of the system. It governs both analog and digital blocks of the ASIC. The jitter of the clock has direct impact on the noise floor of the accelerometer and the sensitivity of the clock to temperature is translated into the temperature sensitivity of the bias. Special design is necessary to ensure that the oscillator is of a quality that supports the navigation grade performance of the accelerometer.

- *Supply voltage regulation*: Stability and low noise of both reference voltage used in the AFE and high voltage used for generating electrostatic force is crucial for achieving designed bias and scale factor stability. The

design of regulation schemes for those voltages needs special attention.

- *Mechanical design of the sensor*: Mechanical design of the MEMS device is challenging and many aspects need to be considered in order to achieve the necessary stability and dynamic range at the system level. Since the thermo-mechanical noise of the MEMS device will appear at the output without much noise shaping, precautions were taken at the early design stages for making this noise contribution as small as possible. The suspension of the proof mass design guarantees effective modal isolation of the sensing mode to avoid unwanted mechanical cross-talks. The metal layer of the MEMS device has a symmetric topology to ensure matched impedance at sensing and driving nodes. Good bias stability cannot be achieved without proper package design and assembly with emphasis on stress and thermal isolation of the MEMS.

C. *Closed-loop accelerometer measurement results*

The initial measurement results from MAXL-CL-3030 accelerometer, shown in [9], already reveal the great potential of the described concept. In this paper we demonstrate the most updated measurement results taken from MAXL-CL-3030 accelerometer with improved ASIC.

- *Single bit stream PSD analysis*: The most reliable indicator of the proper operation of the closed-loop system is the single bit stream PSD plot, presented in Fig. 11. Using the scale factor, calculated from the tumble test, we present the PSD plot with the y axis in µg/Hz$^{0.5}$ units. The scale factor enables the estimation of the maximum feedback acceleration by (9).

$$a_{\max} = 1/SF. \qquad (9)$$

The typical value for the scale factor is around 0.025 bit/g, giving typical maximum feedback acceleration around 40g. In order to ensure reliable operation, sensors full scale is stated as 30 g. From Fig. 11 a noise floor of about 13 µg/Hz$^{0.5}$ is measured. Considering 30g full scale, this is effectively 127 dB dynamic range.

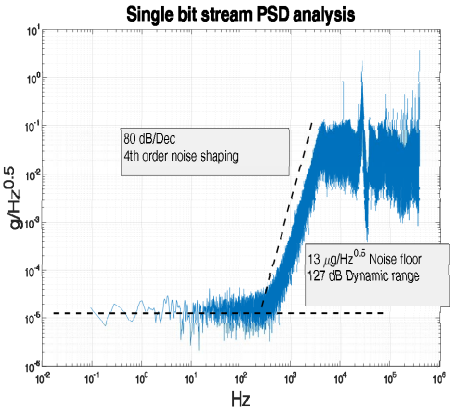

Fig. 11. Single bit stream PSD analysis

In addition, a good verification of the digital compensator's proper functionality is the 80 dB/Dec noise shaping, confirming the 4th order sigma-delta modulation.

- *Allan variance analysis*: The oversampled single bit stream is filtered, to avoid aliasing of high frequency noise to the band of interest, and decimated to get a high resolution digital output signal. The designed bandwidth of the sensor is 300 Hz. The Allan variance analysis is applied to the decimated data in order to verify the decimation algorithm and to gain understanding of the sensors noise performance.

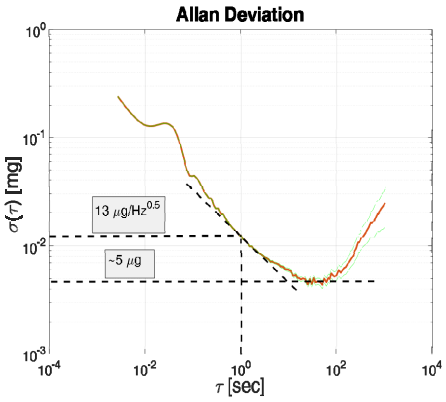

Fig. 12. Allan variance plot on 1 hour decimated data

Fig. 12 shows the Allan variance plot calculated from 1 hour decimated data. The noise floor, calculated from the plot, is in correlation with the result received from the single bit stream PSD analysis, confirming the validity of the filtering and decimation algorithm. Additionally, the minimum value of the Allan variance plot is 5 µg corresponding to about 8 µg flicker noise.

- *Short term stability*: Fig. 13 shows the data acquired from three MAXL-CL-3030 sensors during a 25 hour period with controlled ambient temperature. The plot also shows the change in the ambient temperature during the test, measured by a temperature sensor of one of the tested accelerometers.

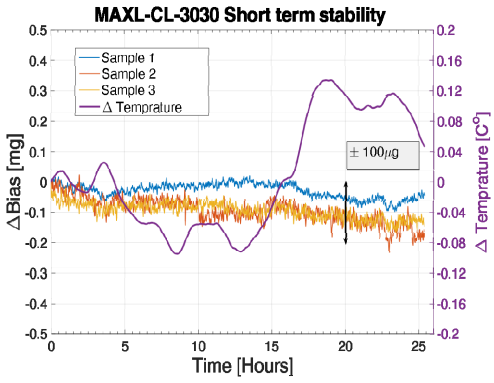

Fig. 13. Short term stability

- *Temperature sensitivity*: The temperature sensitivity measurement of MAXL-CL-3030 accelerometers has been performed under three consecutive -40°C to +85°C temperature cycles. During the test the temperature rate of change was 1°C/min with 30 minute dwelling at -40°C and at +85°C. The sensors were in a vertical static position, so the results represent combined bias and scale factor sensitivity.

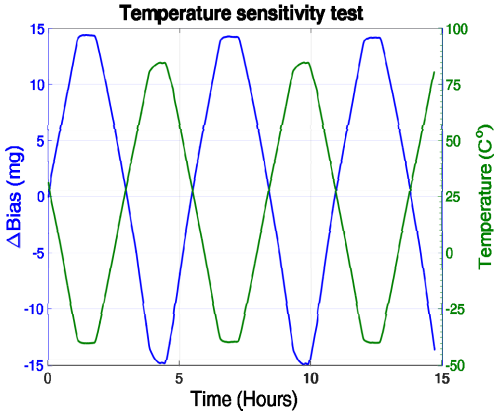

Fig. 14. Temperature sensitivity measurement data

Fig. 14 shows the data of the temperature sensitivity test in time domain. The acceleration and temperature outputs are presented. Fig. 15 shows uncompensated output of two accelerometers during three described above temperature cycles. And finally, Fig. 16 shows the result of 3rd order compensation of the two accelerometers, revealing a residual error of ±250 µg.

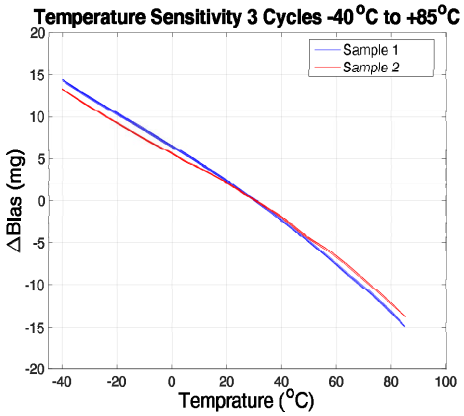

Fig. 15. Accelerometer output vs. temperature

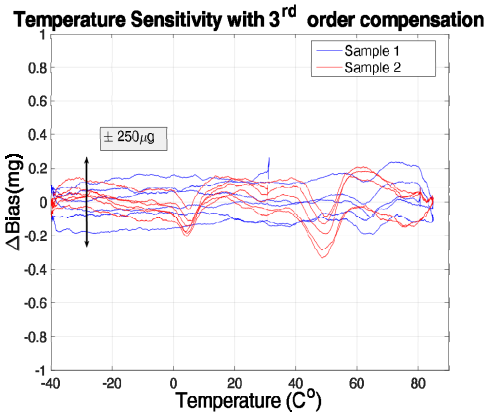

Fig. 16. Temperature sensitivity with 3rd order compensation

- *Vibration*: The VRE of the accelerometer was evaluated under 5 g RMS random vibration in the 20 Hz to 2000 Hz frequency range. Fig. 17 shows the results of the test.

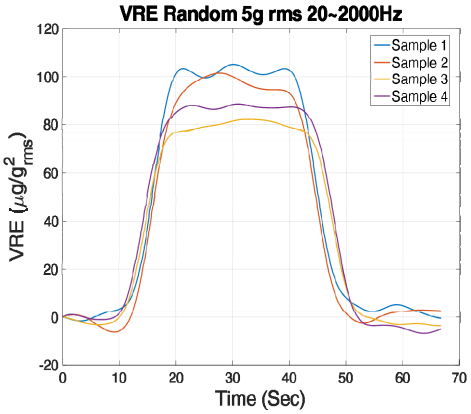

Fig. 17. VRE under 5g random vibration

- *Linearity*: MAXL-CL-3030 accelerometers went through precise centrifuge testing. The purpose of the test was to verify the 30 g sensing range and to evaluate the sensors scale factor linearity. The sequence of the applied accelerations can be seen in Fig. 18. The calculation of the nonlinearity error is performed using linear approximation based on 0 g and 1 g measurements as a reference. The nonlinearity error in g units is shown in Fig. 19, the red dashed line indicates the 0.1% error limit. In total six units were tested, all of them showed 0.1% typical nonlinearity in 27 g range.

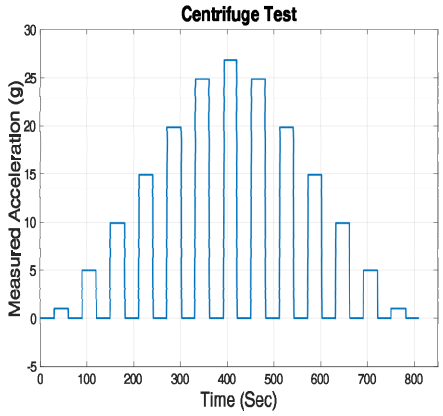

Fig. 18. Centrifuge test row data

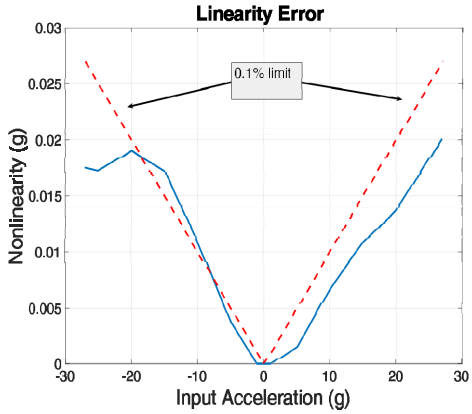

Fig. 19. MAXL-CL-3030 nonlinearity error

CONCLUSION

We have presented a matured technology for open-loop and closed-loop MEMS accelerometers, realized using in-plane bulk micro-machining fabrication process.

Our MAXL-OL-2000 open-loop accelerometer series demonstrate performance that meets the requirements of tactical grade guidance systems. Furthermore, our MAXL-CL-3030 30 g closed-loop MEMS accelerometer, described in this paper, exhibits navigation grade performance with excellent bias and scale factor stability over temperature, 0.1% of full range linearity error, and <100 $\mu g/g^2_{rms}$ VRE.

The results presented in the paper confirm that MEMS accelerometers can compete with traditional electro-mechanical accelerometers in the most demanding applications.

ACKNOWLEDGMENT

The authors would like to thank the Institute of Microelectronics, A*STAR (Singapore) for participation in system and ASIC design, and Tower/Jazz (Israel) for collaboration in process development and fabrication.

REFERENCES

[1] M. Guler and S. Ertugrul, "Measuring and Transmiting Vital Body Signs Using MEMS Sensors," RFID Eurasia, 2007 1st Annual, pp, 1-4, 2007.

[2] S.A.P. Haddad, R.P M Houben and W.A. Serdijin, " The Evolution of Paceemakers", IEEE Eng. Med. Bio. Mag, vol. 25, pp. 38 – 48, 2006.

[3] J-M Stauffer, O. Dietrich, B. Dutoit, "RS9000, a Novel MEMS Accelerometer Family for Mil/Aerospace and Safety Critical Applications", IEEE/ION PLANS, 2010.

[4] Kevin T.C. Chai et al., "118-dB Dynamic Range, Continuous-Time, Open-Loop Capacitance to Voltage Converter Readout For Capacitive MEMS Accelerometer", IEEE Asian Solid-State Circuits Conference 13-4,2010

[5] H. Külah, J. Chae, N. Yazdi, K. Najafi, "Noise Analysis and Characterization of a Sigma-Delta Capacitive Microaccelerometer", IEEE J. of Solid-State Circuits, Vol. 41, No. 2, pp. 352-360, February 2006

[6] J. Wu and L. R. Carley, "Electromechanical ΔΣ Modulation With High-Q Micromechanical Accelerometers and Pulse Density Modulated Force Feedback", IEEE Transaction on Circuits and Systems – I, vol. 53, pp. 274-288, 2006.

[7] P/ Zwahlen, Y. Dong, A-M Nguyen, F. Rudolf, J-M Stauffer, "Breakthrough in High Performance Inertial Navigation Grade Sigma-Delta MEMS Accelerometer", IEEE/ION PLANS, 2012.

[8] C. Wang, K.T.C Chai, V. Suplin, D. Nuttman, and Minku Je, "Reconfigurable Closed-Loop Digital ΔΣ Capacitive MEMS Accelerometers for Wide Dynamic Range, High Linearity Applications", International Journal of Information and Electronics Engineering, Vol. 3, No 1, pp 44 – 48, 2013.

[9] A. Feingold, B. Grinberg, "In-Plane Bulk-Micromachinning Fabrication of High Dynamic Range Tactical Grade Open Loop and Closed Loop MEMS Accelerometers", IEEE Sensors 2015, pp 287 – 290, 2015.